The Lighthouse Journal of Natural Sciences, Vol. 01, Issue 01, Summer 2022, pp. 21-30

Utilization of 0D Perovskite to the 3D Organometal Halide Perovskite: Improved Morphological, Optical, and Structural Properties

Irfan Ullah[1], Waqas Rahim[1], Muhammad Sajid[1], Muhammad Idrees[1], Aqib Javed[1], Abbas Khan[1], Arsalan Khan[1], Muhammad Asad[1], Nasir Ali[1], Sanam Attique[2]

ABSTRACT

Albeit low efficiency of lower-dimensional perovskites are still game-changer; when they are used with 3D perovskites. Numerous factors are responsible for efficient photovoltaic devices based on organometal halide perovskites. Among them, better film morphology and extended environmental stability are critical parameters, governing the photovoltaic performance of a device. The present researche has utilized lower-dimensional perovskites, i.e., $DA_{0.1}Cs_{2.9}Bi_2I_9$ (0D) into triple-cations organometal halide perovskite, i.e., $CsFAMAPbI_3$ (3D) to fabricated compact films in the ambient environment without pre-heating the substrate. It is revealed by various characterization results that the prepared 0D/3D perovskites films exhibited better film morphology, improved crystallinity, and optoelectronic properties. The 0D perovskites shield the 3D perovskites from moisture ingress consequently, the final product remains environmentally stable. This study can provide a pathway toward the ambient fabrication of high-quality perovskite thin films for highly efficient optoelectronic devices.

Keywords: *$DA_{0.1}Cs_{2.9}Bi_2I_9$; $CsFAMAPbI_3$; 0D/3D perovskites; Thin films*

INTRODUCTION

Organometal halide perovskites are emerging as a promising material for solar energy harvesting and other optoelectronic applications [1-5]. Its peculiar optoelectronic properties; including higher photoabsorption and photoemission, longer carrier diffusion length, and weaker exciton binding boosted the photoconversion efficiency of perovskites solar cells to 26% in only 9 years [1-3, 6-9]. Although their power conversion efficiency is on par with the conventional silicon-based solar cells; it is still way lower than the theoretically predicted limit for single-junction solar cells [10, 11]. Many factors govern the performance of photovoltaic devices; for example, compact pinholes-free perovskite films, uniform surface morphology, and better crystallinity are ideal to ensure maximum efficiency. In addition, perovskite material is very sensitive to the ambient environmental condition, e.g., humidity, high temperature, and UV light.

Therefore, it is challenging to guarantee a compact high-quality perovskite thin film with a larger grain size while using simple solution processability in the ambient environment. Many techniques including spray paralysis, solvent engineering, hot costing, etc. are utilized

[1] Government Degree College Thana, District Malakand, Pakistan, **Coresponding Author's Email: nasirphysicist@yahoo.com**

[2] Institute for Composites Science and Innovation (InCSI), School of Material Science and Engineering, Zhejiang University, Hangzhou 310027, PR China

Manuscript Submitted: May 10, 2022
Manuscript Accepted: June 20, 2022

to fabricate compact perovskites thin films with larger grain sizes [12-14]. Liang et al. [12] fabricated compact perovskite thin-film via spray paralysis under ambient conditions (with 50% humidity) without post-annealing. The prepared thin films exhibited larger grain sizes about micrometer size, which covered the substrate completely.

The heterojunction photovoltaic devices showed a power conversion efficiency of 7.89%, which was expected to further increase with post-annealing. Likewise, Gedamu et al. [13] fabricated pinholes-free perovskites ($CH_3NH_3PbI_{3-x}Cl_x$) thin films with higher substrate coverage (~99.97%) and larger crystals (> 5 µm) by utilizing solvent engineering under ambient environmental conditions. Solar cell devices based on those films demonstrated a power conversion efficiency of 14%, which was attributed to the larger grain size and denser film morphology of the film.

Lower dimensional perovskites are found to be relatively stable than their 3D counterparts; for example, 2D perovskites exhibited better environmental stability than bulk perovskites [15, 16]. Similarly, dodecylammonium chloride (DCl) utilized and enabled the fabrication of the perovskite thin films due to the formation of hybrid 2D/3D perovskites in the ambient environment [15]. The prepared films not only showed better crystallinity, optoelectronic properties, film morphology, and environmental stability than the pure 3D perovskites, but also exhibited an enhanced device performance.

The improved environmental stability of the hybrid perovskites can be attributed to the 2D perovskites being relatively more hydrophobic and longer chained organic cations acting as a shield again environmental factors [17, 18]. Moreover, along with other excellent optoelectronic properties, 0D Bi-based perovskites ($Cs_3Bi_2I_9$) also demonstrated excellent environmental stability than the conventional organolead-based perovskites. For example, the excellent environmental stability of 6 months for $Cs_3Bi_2I_9$ thin films has been reported [19].

Inspired by the above studies; the researchers herein utilized first a minute amount of dodecylammonium chloride into the 0D Bi-based perovskites ($Cs_3Bi_2I_9$) to prepare $DA_{0.1}Cs_{2.9}Bi_2I_9$ (DCBI). Subsequently, a small amount of DCBI is added to the triple cations-based 3D perovskites (i.e. $CsFAMAPbI_3$) to prepare 0D/3D perovskites i.e. ($DCBI_x$.$CsFAMAPbI_3$).

Thin films based on this perovskite compound are characterized by optical and electron microscopies; exhibited excellent coverage with compact grain boundaries. The films were also characterized by X-ray diffraction analysis, which revealed an improved crystallinity of the films as compared with pure $CsFAMAPbI_3$ films. The existence of vertically-oriented 0D perovskite crystals among the 3D perovskite crystals not only endows the 3D perovskites with better environmental stability but also helps in charge transportation.

METHODOLOGY

All reagents, cesium iodide (CsI), bismuth iodide (BiI_3), lead iodide (PbI), dodecylammonium (DCA), hydrochloric acid (HCl, 37 wt% in H_2O), methylammonium iodide (MAI), formamidinium iodide (FAI), dimethylformamide (DMF), and indium tin oxide (ITO) glass substrates were obtained from Aladdin, China. All of the reagents were used as received.

Synthesis of precursor solutions

To synthesize dodecylammonium chloride, 1 equivalent of dodecylammonium was thoroughly dissolved in ethanol (at 0 °C) and a slightly excessive amount of HCl (i.e., 1.1 equivalent) was titrated into the above solution (with constant stirring for 2 h at 0 °C). The dried solution turned into a white powder (after evaporation). Afterward, the powder washing was done for several times using diethyl ether. The powder was then filtered followed by drying at 50 °C for 24 hours. The obtained white powder of the dodecylammonium chloride will be used as a precursor of dodecylammine.

Preparation of $Cs_3Bi_2I_9$

To prepare the 0D $Cs_3Bi_2I_9$ (CBI) precursor solution, 1.5 mM of CsI and 1 mM BiI_3 were completely dissolved in DMF under constant stirring for 2 hours (70 ℃). After the species in the solution were fully dissolved, a 0.45 µl organic filter was used to filter out the solution.

Preparation of $DA_{0.1}Cs_{2.9}Bi_2I_9$ and $FAMAPbI_3$

To prepare $DA_{0.1}Cs_{2.9}Bi_2I_9$, a 0.1 mM of dodecylammonium chloride was added to the CBI solution and stirred again for 6 hours. Afterward, the solution was filtered again with a 0.45 µl organic filter.

Similarly, to prepare the 3D $FAMAPbI_3$ precursor, 0.7 mM of MAI, 0.1 mM of CsI, and 0.2 mM of FAI were fully dissolved in DMF by means of stirring for 12 hours (70℃). Upon full dissolution, the precursor was filtered with a 0.45 µl organic filter.

Preparation of 0D/3D Perovskites

To synthesize mixed 2D/3D perovskites (DA.$Cs_3Bi_2I_9$ and $FAMAPbI_3$), 5% addition of $DA_{0.1}Cs_{2.9}Bi_2I_9$ to the $FAMAPbI_3$ and let it stirred for 6 hours to prepare 0D/3D perovskites. This solution will be used for film fabrication, which will be further characterized by optical microscopes, scanning electron microscopy, and X-ray diffraction analysis.

Preparation of thin films

Before film fabrication, the ITO glass was sonicated (10 min) in de-ionized water, acetone, and ethanol. Each time after sonication, the glass substrates were dipped in hot water (~ 90 ℃) and dried with nitrogen gas. The substrates were finally treated with UV-Ozone to remove all the organic species from the surface. Subsequently, 70 µl of the precursor solution was dropped genteelly on the already spinning glass substrate (3500 rpm) and allowed to rotate for 1 minute. Afterward, the substrate was quickly transferred to the hot plate and annealed at 120 ℃ for 5 minutes while covered with a glass dish.

Characterization Techniques

Photoluminescence (PL) analysis was done by Andor SR-500i-B1 spectrograph FLS-920 and fluorescence spectrometer from Edinburgh Instrument with 535 nm laser beam as incident radiation. UV absorption were done by Carry 5000 UV–VIS-NIR spectrometer from Agilent Technologies. For the investigation of the films surface morphology; a scanning electron microscope (SEM) from Hitachi S4800 was used. X-ray diffraction (XRD) measurements were performed by Empyrean Alpha-681 X-Ray Diffractometer from PANalytical. The water contact angle was measured through CAM200 optical contact-angle meter (KSV Co.Ltd.).

DISCUSSION AND ANALYSIS

Figure 1a shows the absorption measurement plots of both 3D perovskite thin films. A strong absorption slope near 800 nm, can be attributed to the absorption characteristics of the 3D perovskites. In comparison to the pure 3D perovskite, the 0D/3D perovskites exhibited more steeper absorption slope, which is indicative of the films with fewer defects and better crystallinity [20].

An optical energy bandgap is an important parameter to efficiently absorb the sunlight and convert it into an electrical current. The present study calculated the optical energy bandgaps for both puer 3D and 0D/3D perovskites from their Tauc's plots, as shown in **Figure 1b**. The onset wavelength of the absorption slope of the pure 3D perovskites in the Tauc plot indicates a bandgap of ca. 1.51 eV, which is closer to optimum bandgap of single-junction solar cell and is consistent with the previous studies [21]. In contrast to this, the 0D/3D perovskite showed a slightly wider energy bandgap of 1.53 eV, which can be attributed to the existence of the lower dimensional (0D) perovskites [20].

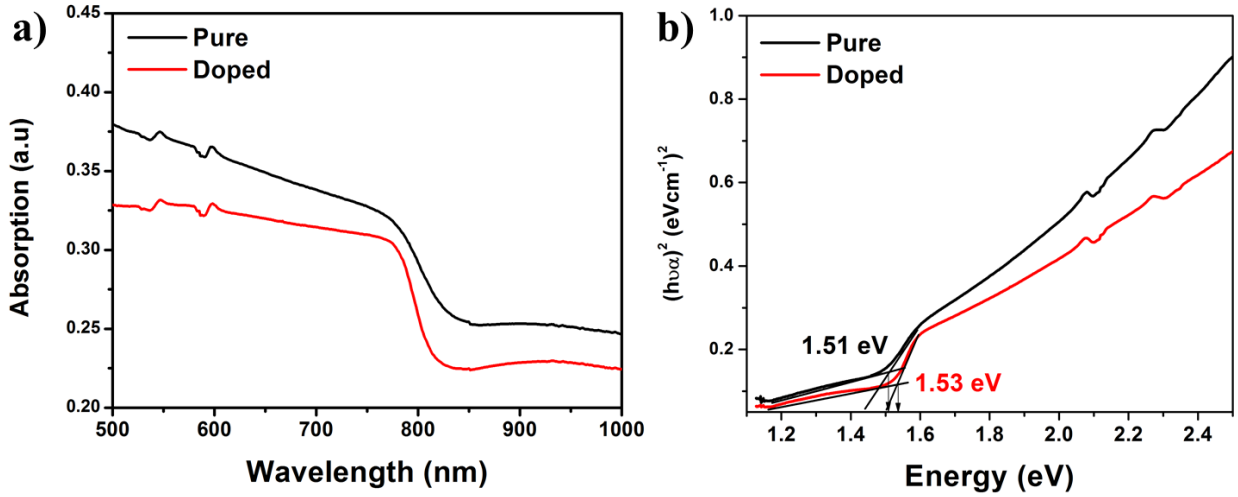

Figure 1 (**a**) Absorption plots for pure and doped perovskite thin films. (**b**) Tauc plot of pure and doped perovskite films for energy bandgap calculations.

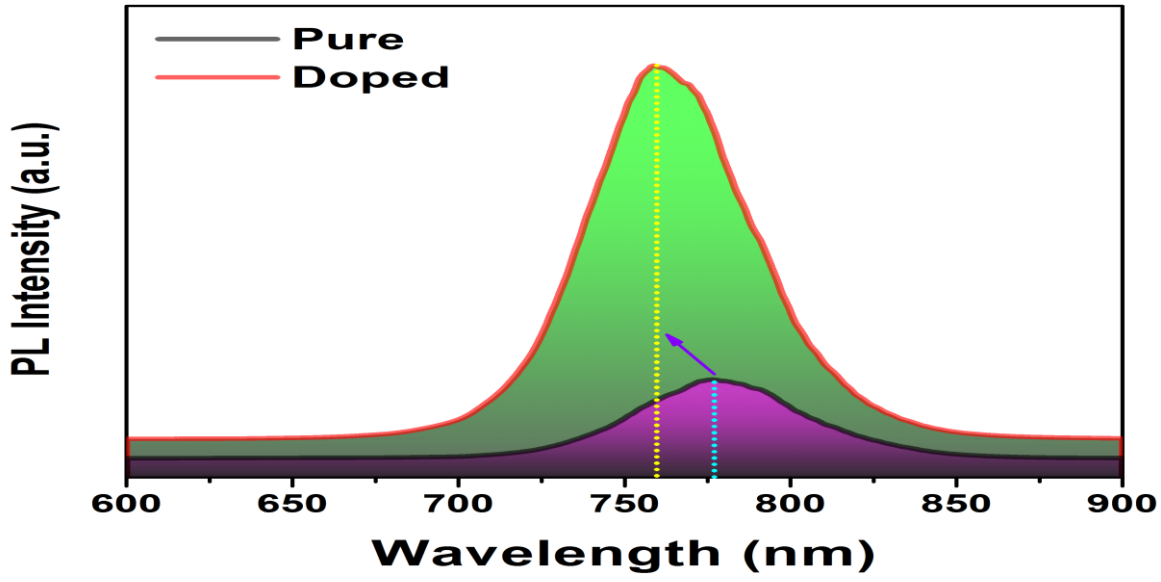

Figure 2 Photoluminescence spectra of the pure and doped perovskite thin films. The dotted lines and an arrow are the guideline to the eye to indicate the blue shift in the PL spectra.

Similarly, photoluminescence (PL) characterizations of the pure and doped samples were carried out, as shown in **Figure 2**. Pure 3D perovskite thin-film shows wider and less intense PL characteristics with a peak near 800 nm. While 0D/3D perovskites show strong and narrow PL characteristics with a peak slightly blue-shifted. The blue shift in the PL peak is consistent with increased energy bandgap (calculated from absorption spectrum) and is attributed to the existence of the lower dimensional (0D) perovskites. The PL peak exhibit a smaller full-width maxima, indicating the better crystallinity and lesser defects sites in the 0D/3D perovskites films and is consistent with the steeper absorption slope in **Figure 1a**.

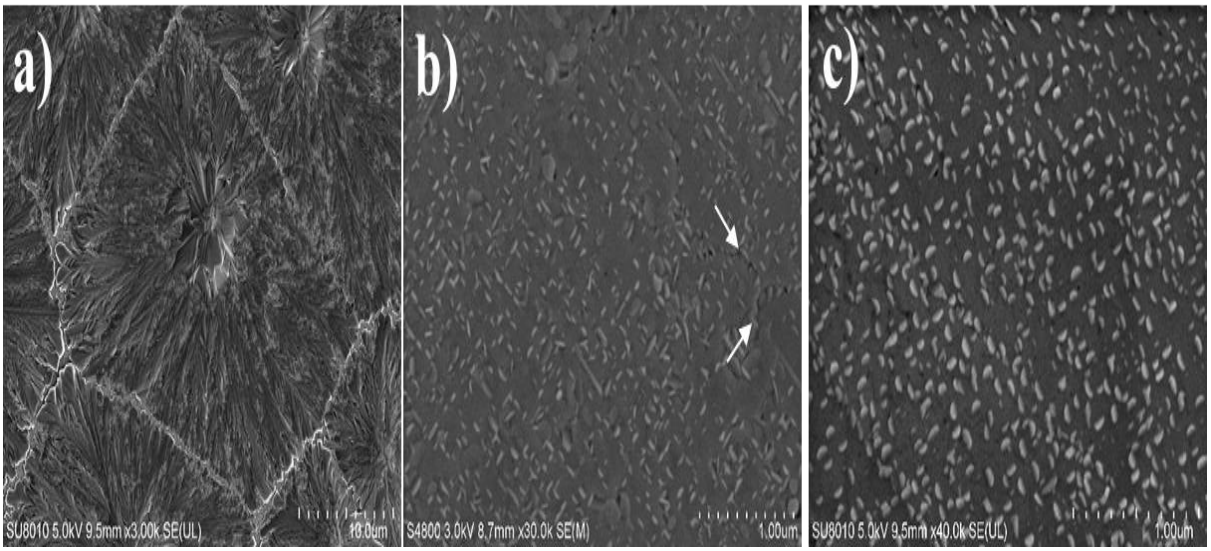

Figure 3 Scanning electron microscopic images of the pure (**a**) and (**b**, **c**) doped perovskite films. The arrows indicate the filling of the 0D perovskite sheets filled up in the grain boundaries. Scale bars: (**a**) 10 µm, (**b**) 1 µm, and (**c**) 1 µm.

To examine the surface morphology of the pure 3D and doped 0D/3D perovskites films, scanning electron microscopy (SEM) was performed, as shown in **Figure 3**. Pure 3D perovskites show large crystal domains with rough film morphology and defined domain boundaries, as shown in **Figure 3a**.

In contrast to this, 0D/3D perovskites showed smoother morphology with small hexagonal crystals vertically embedded into the 3D perovskite matrix, as shown in **Figures 3b** and **3c**. The smoother film morphology could be helpful for better contact between charge transporting material, leading toward better charge transportation. Also, the vertically oriented 0D perovskite crystals could have synergistic advantages, i.e., i. due to their hydrophobic nature, they act as shields against the moisture ingress to the main 3D perovskite matrix; ii. due to their vertical orientation to the substrate, they could fasten the charge transportation [22].

From the SEM images, larger crystal domains can be observed, which may be formed by the combination of a large number of crystallites. Such a large crystal domain could be useful to reduce the grain boundary, which leads to lesser carriers' recombination losses. Also, it provides more freedom to the exciton electron-hole pair to move across the grains and mitigates the defects in the sample. Moreover, due to their smaller surface-to-volume ratio, films with bigger domains are more environmentally stable [23].

In addition, the 0D perovskite crystals have filled up the grain boundaries (as shown in **Figure 3c**), hence minimizing the defect concentration in the film. Such high-quality compact films are favorable for increased PV characteristics and decreased hysteresis losses [24].

To confirm whether these small vertically oriented crystals on the surface of the larger grain are 0D Bi-based perovskites or not; energy-dispersive x-ray spectroscopy (EDX) analysis was carried out. The elemental map of the EDX analysis (shown in **Figure 4**) showed a signature of bismuth and iodine along with other elements (given in table **Figure 4**).

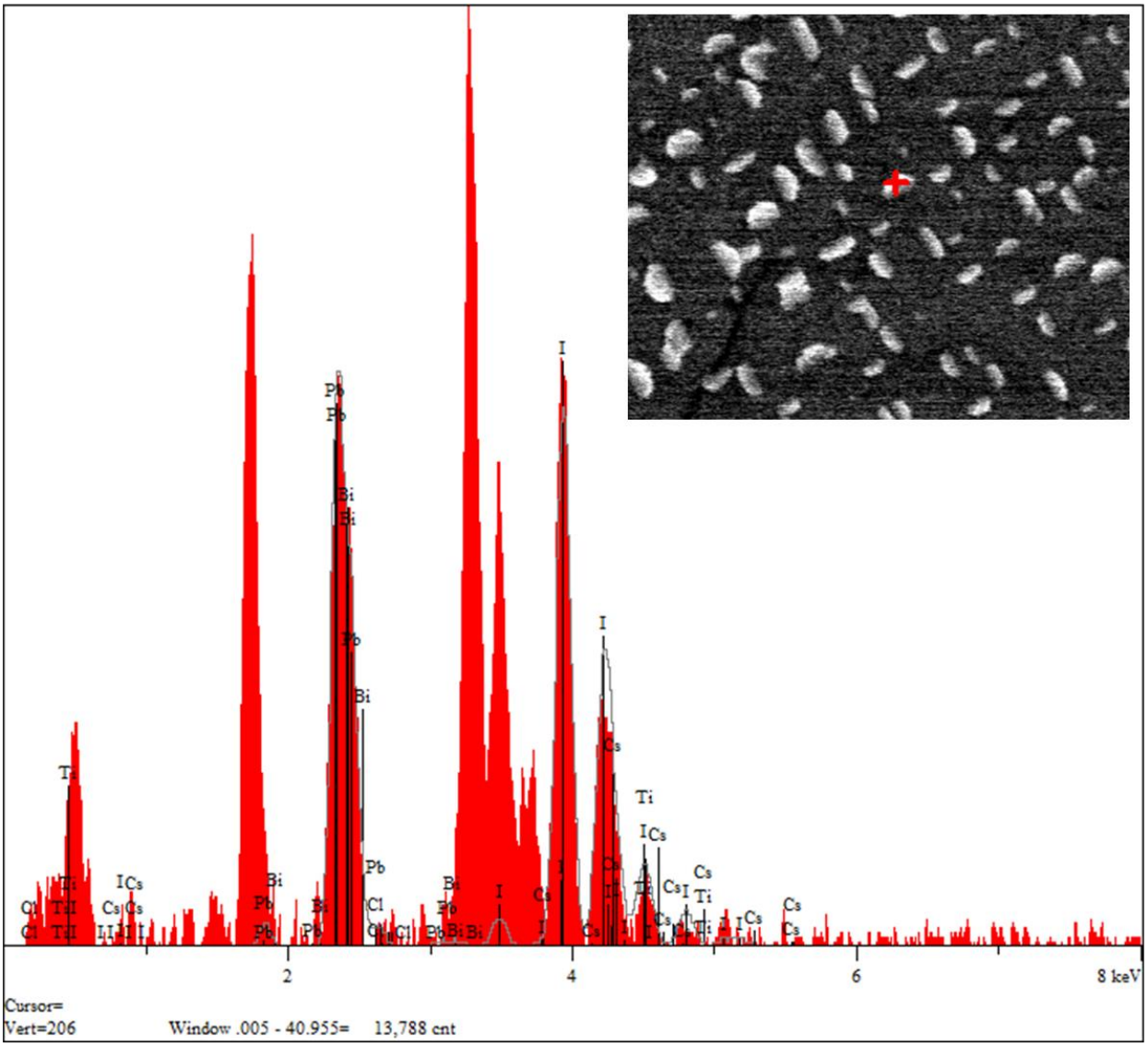

Elt.	Line	Intensity (c/s)	Atomic %	Atomic Ratio	Conc	Units	Error 2-sig	MDL 3-sig	
Cl	Ka	.00	.000	.0000	.000	wt.%	.000	.000	
Ti	Ka	.00	.000	.0000	.000	wt.%	.000	.000	
I	La	153.18	47.172	1.0000	35.327	wt.%	2.215	1.966	
Pb	La	6.48	45.736	.9696	55.926	wt.%	24.213	30.349	
Bi	La	.64	7.092	.1503	8.746	wt.%	31.594	47.177	
			100.000		100.000	wt.%			Total

Figure 2 EDX mapping of the small sheet-like crystals (top) and corresponding elemental chart (bottom). The inset of the figure is the SEM image of the selected area, which was used for EDX characterization.

The improved crystallinity of the 0D/3D perovskite films was also justified by their XRD analysis. **Figure 5a** shows the XRD patterns of the pure 3D perovskites (bottom) as well as 0D/3D perovskites (top and middle). It can be observed from the pure 3D perovskites pattern that the peaks are very faint showing poor crystallinity and orientation of the crystals. On the other side, the XRD pattern of the 0D/3D perovskites (middle) shows significantly intense peaks, indicating its superior crystallinity and preferred orientation perpendicular to the substrate. The peaks near 14° and 28° (designated with stars and diamond symbols) are representing the reflection from the (001) and (002) planes of the cubic phased perovskite crystals [15]. All of the peaks exhibit narrow full-width maxima, indicating the larger size of the crystals. The top of **Figure 5a** shows the XRD pattern of the same sample after being exposed to the ambient environment for 2 weeks.

Almost no change is observed in the XRD pattern of the sample, indicating that the samples retained their crystallinity even after exposure to the ambient conditions. The improved environmental stability is attributed to the inclusion of the lower dimension perovskites as well as to the compactness of the film.

The existence of the small peak (**Figure 5b**, designated with a sphere) near the 8° is attributed to the formation of the 2D perovskites due to the reaction of the DACl with the leftover PbI_2. Such peaks are also previously observed for the 2D/3D perovskites [15]. The increased crystal size can also be observed from the deviation of the main 3D perovskites peaks towards lower angles, which usually occurred with the shrinkage of the crystal size.

Furthermore, the crystallites size for the doped samples is calculated using D. Scherrer's equation formula: $d = K\lambda/\beta Cos\theta$ [25]. Where d is crystallite size, K is Scherrer's constant (i.e., 0.94), λ is x-ray's wavelength (i.e., 1.5406 Å for CuKα)), β is full-width of the half maximum (FWHM), and θ is the Bragg's angle in degrees. By using FWHM = 0.07222 (calculated from the intense diffraction peak), θ = 0.9925, the crystallite size is calculated to be 2.02 nm. The crystallite size is much smaller than the crystal domains or grains that are shown in the SEM images, which indicates that the crystal domains are composed of a large number of crystallites.

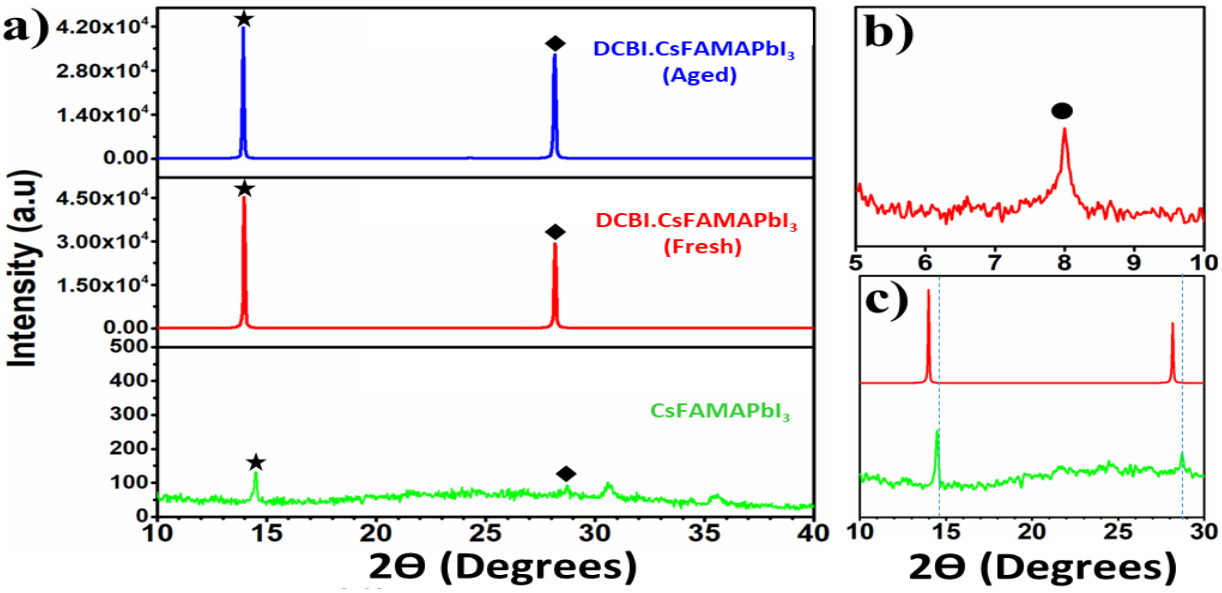

Figure 5 X-ray diffraction analysis of the DCBI doped CsFAMAPbI$_3$ perovskites thin film: (**a**) Pure CsFAMAPbI$_3$ (bottom), freshly doped with DCBI (middle), and aged doped with DCBI (top). Stars and diamonds represent the main 3D perovskite peaks. (**b**) The visualization of the peak is due to the formation of the 2D perovskites. (**c**) The deviation of the main XRD peaks towards a smaller angle.

CONCLUSION AND RECOMMENDATIONS

The researchers combined a 3D perovskite (CsFAMAPBI$_3$) with a dodecylammonium chloride doped 0D perovskite to prepare 0D/3D perovskites. Thin films based on such perovskite exhibited larger grains with compact grain boundaries. The surface morphology of the films was studied using scanning electron microscopy. The improved crystallinity of the 0D/3D perovskite films was justified by XRD analysis. Optical absorption and PL spectra showed the typical characteristics of the 3D perovskites. Along with better crystallinity, the prepared 0D/3D perovskites exhibited improved environmental stability. It is believed that these high-quality, pinholes-free, and compact perovskite films with larger grain sizes will play a vital role in the improvement of the performance of the next generation of perovskite-based optoelectronic devices.

Acknowledgment

We acknowledge funding from Zhejiang Provincial Natural Science Foundation of China (LR19E010001) and the National Science Foundation of China (51702283 and 51871246).

REFERENCES

1. Yang, W. S., Park, B. W., Jung, E. H., Jeon, N. J., Kim, Y. C., Lee, D. U., ... & Seok, S. I. (2017). Iodide management in formamidinium-lead-halide–based perovskite layers for efficient solar cells. *Science*, *356*(6345), 1376-1379.

2. Correa-Baena, J. P., Saliba, M., Buonassisi, T., Grätzel, M., Abate, A., Tress, W., & Hagfeldt, A. (2017). Promises and challenges of perovskite solar cells. *Science*, *358*(6364), 739-744.

3. Kojima, A., Teshima, K., Shirai, Y., & Miyasaka, T. (2009). Organometal halide perovskites as visible-light sensitizers for photovoltaic cells. *Journal of the american chemical society*, *131*(17), 6050-6051.

4. Sai Bai, Yizheng, and J.F. Gao. (2015). *Organometal Halide Perovskites for Photovoltaic Applications*, in *Advanced Functional Materials*. p. 535-566.

5. Zhang, W., Eperon, G. E., & Snaith, H. J. (2016). Metal halide perovskites for energy applications. *Nature Energy*, *1*(6), 1-8.

6. Saparov, B., & Mitzi, D. B. (2016). Organic–inorganic perovskites: structural versatility for functional materials design. *Chemical reviews*, *116*(7), 4558-4596.

7. *Best Research-Cell Efficiency Chart*.https://www.nrel.gov/pv/cell-efficiency.html.

8. Jeong, J., Kim, M., Seo, J., Lu, H., Ahlawat, P., Mishra, A & Kim, J. Y. (2021). Pseudo-halide anion engineering for α-FAPbI3 perovskite solar cells. *Nature*, *592*(7854), 381-385.

9. *Chart of Best Research-Cell Efficiencies*.Retrieved June 4, 2021 from http://www.nrel.gov/pv/assets/images/efficiency_chart.jpg.

10. Ma, L., Ju, M. G., Dai, J., & Zeng, X. C. (2018). Tin and germanium based two-dimensional Ruddlesden–Popper hybrid perovskites for potential lead-free photovoltaic and photoelectronic applications. *Nanoscale*, *10*(24), 11314-11319.

11. Reshi, H. A., & Zargar, R. A. (2018). Perovskite solar cells: the challenging issues for stable power conversion efficiency. *Recent Dev. Optoelectron. Devices*, *117*.

12. Liang, Z., Zhang, S., Xu, X., Wang, N., Wang, J., Wang, X., & Ding, J. (2015). A large grain size perovskite thin film with a dense structure for planar heterojunction solar cells via spray deposition under ambient conditions. *RSC advances*, *5*(74), 60562-60569.

13. Gedamu, D., Asuo, I. M., Benetti, D., Basti, M., Ka, I., Cloutier, S. G., & Nechache, R. (2018). Solvent-antisolvent ambient processed large grain size perovskite thin films for high-performance solar cells. *Scientific reports*, *8*(1), 1-11.

14. Nie, W., Tsai, H., Asadpour, R., Blancon, J. C., Neukirch, A. J., Gupta, G., & Mohite, A. D. (2015). High-efficiency solution-processed perovskite solar cells with millimeter-scale grains. *Science*, *347*(6221), 522-525.

15. Ali, N., Wang, X., Rauf, S., Attique, S., Khesro, A., Ali, S., & Wu, H. (2019). Enhanced stability in cesium assisted hybrid 2D/3D-perovskite thin films and solar cells prepared in ambient humidity. *Solar Energy*, *189*, 325-332.

16. Ali, N., Rauf, S., Kong, W., Ali, S., Wang, X., Khesro, A., & Wu, H. (2019). An overview of the decompositions in organo-metal halide perovskites and shielding with 2-dimensional perovskites. *Renewable and Sustainable Energy Reviews*, *109*, 160-186.

17. Zhang, X., Wu, G., Fu, W., Qin, M., Yang, W., Yan, J., & Chen, H. (2018). Orientation regulation of phenylethylammonium cation based 2D perovskite solar cell with efficiency higher than 11%. *Advanced Energy Materials*, *8*(14), 1702498.

18. Yao, K., Wang, X., Xu, Y. X., Li, F., & Zhou, L. (2016). Multilayered perovskite materials based on polymeric-ammonium cations for stable large-area solar cell. *Chemistry of Materials*, *28*(9), 3131-3138.

19. Khadka, D. B., Shirai, Y., Yanagida, M., & Miyano, K. (2019). Tailoring the film morphology and interface band offset of caesium bismuth iodide-based Pb-free perovskite solar cells. *Journal of Materials Chemistry C*, *7*(27), 8335-8343.

20. Ali, N., Attique, S., Rauf, S., Wang, X., Khesro, A., Ali, S., & Wu, H. (2020). The effect of dodecylammonium chloride on the film morphology, crystallinity, and performance of lead-free Bi-based solution-processed photovoltaics devices. *Solar Energy*, *207*, 1356-1363.

21. Bi, C., Shao, Y., Yuan, Y., Xiao, Z., Wang, C., Gao, Y., & Huang, J. (2014). Understanding the formation and evolution of interdiffusion grown organolead halide perovskite thin films by thermal annealing. *Journal of Materials Chemistry A*, *2*(43), 18508-18514.

22. Zhang, X., Wu, G., Yang, S., Fu, W., Zhang, Z., Chen, C., & Chen, H. (2017). Vertically oriented 2D layered perovskite solar cells with enhanced efficiency and good stability. *Small*, *13*(33), 1700611.

23. Attique, S., Ali, N., Khatoon, R., Ali, S., Abbas, A., Yu, Y., & Yang, S. (2020). Aqueous phase fabrication and conversion of Pb (OH) Br into a CH 3 NH 3 PbBr 3 perovskite and its application in resistive memory switching devices. *Green Chemistry*, *22*(11), 3608-3614.

24. Tang, Z., Bessho, T., Awai, F., Kinoshita, T., Maitani, M. M., Jono, R., & Segawa, H. (2017). Hysteresis-free perovskite solar cells made of potassium-doped organometal halide perovskite. *Scientific Reports*, *7*(1), 1-7.

25. Ali, N., Bi, G., Khesro, A., Khan, M., Lang, J., Samreen, A., & Wu, H. (2018). Hybrid AgNPs/MEH-PPV nanocomplexes with enhanced optical absorption and photoluminescence properties. *New Journal of Chemistry*, *42*(23), 18991-18999.